



## Research Article

# Dynamics Analysis and Experiment of Novel Compound Dry Separator

Li Hongxi <sup>1</sup>, Zhou Enhui <sup>2</sup>, Zhang Bo,<sup>2</sup> Jiang Haishen,<sup>2</sup> Shen Ling,<sup>3</sup> and Yin Zixin<sup>1</sup>

<sup>1</sup>School of Mechanical and Electronic Engineering, Suzhou University, Suzhou, Anhui, China

<sup>2</sup>School of Chemical, China University of Mining and Technology, Xuzhou, Jiangsu, China

<sup>3</sup>School of Physics, China University of Mining and Technology, Xuzhou, Jiangsu, China

Correspondence should be addressed to Li Hongxi; [lihongxi@cumt.edu.cn](mailto:lihongxi@cumt.edu.cn) and Zhou Enhui; [zeh@cumt.edu.cn](mailto:zeh@cumt.edu.cn)

Received 28 July 2022; Revised 25 August 2022; Accepted 20 September 2022; Published 6 October 2022

Academic Editor: Antonio Batista

Copyright © 2022 Li Hongxi et al. This is an open access article distributed under the Creative Commons Attribution License, which permits unrestricted use, distribution, and reproduction in any medium, provided the original work is properly cited.

China is the world's largest producer and consumer of coal. The method of dry coal beneficiation is a key method of separation technology in the field of coal mining. In this paper, the structure of a novel compound dry separator (NCDS) was revealed. The dynamic characteristics and vibration behavior of the NCDS were studied through theoretical modeling, simulation research, and experimental test methods. The mathematical model and simulation model based on ADAMS of the NCDS were established. The experiment for the NCDS was carried out using the dynamics characteristic testing system. The dynamic curve and spatial trajectory of the NCDS were obtained. The Lissajous figure of displacement indicated that the space motion trajectory of the NCDS was an oblique line. The dynamic characteristics of the NCDS with different rotational speeds were revealed. The effect of eccentricity on the dynamic characteristics of the NCDS was discussed, and the vibration amplitudes increased with the increase of eccentricity. The results showed that the deviation of the simulation data and theoretical data was within 3.75%, and the result of the experiment data and theoretical data was within 6.98%. Through comparison and verification, the theoretical model with high accuracy can accurately calculate the dynamic characteristics of the NCDS before processing and manufacturing. This paper provides a reference for the design and efficient operation of the new compound dry separation machine.

## 1. Introduction

Coal occupies a dominant position in primary energy consumption [1, 2]. China is the world's largest producer and consumer of coal [3, 4]. Coal beneficiation is applied to remove minerals that decrease the value of the coal product, such as carbonate, pyrite, and silicate [5, 6]. Coal beneficiation is a key process for deep processing of raw coal, and it is also the source technology for clean and efficient utilization of coal and the basis for purifying air pollution [7, 8]. The methods of coal beneficiation mainly include wet-beneficiation processes and dry-beneficiation processes [9, 10]. At present, wet beneficiation of coal is extensively used because of its advantages of quality products and high recovery [11]. However, wet coal preparation requires a large amount of water, which is not possible in arid areas. In addition, the moisture content of the final

product of wet coal preparation is very high (up to 12%), making storage and transportation very difficult [12–14].

The overall distribution of coal resources in China is more in the west and less in the east, and more in the north and less in the south. Most of northwest China belongs to the area with extreme water shortages and a cold climate. For the coal resources with abundant reserves in these areas, dry coal preparation technology is urgently needed to process and improve the quality of coal. Dry coal separation has more advantages than wet coal separation [15–17]. Compound dry coal preparation technology is a new coal preparation method suitable for China's national conditions [13, 18].

Currently, the compound dry separator is mainly used for the roughing of thermal and miscellaneous coal and predischarging gangue [19, 20]. The compound dry separator uses pulverized coal contained in the feed as the autogenic medium to form a gas-solid two-phase mixture [21].

Materials are stratified on the separation bed of the separator by the comprehensive action of vibration and wind, and the separation process by density is realized under the action of buoyancy of high-density materials [22, 23]. The research on the design theory and equipment of the compound dry separator provides technical support and equipment support for large coal preparation plants in China, which is of great significance for improving the raw coal selection rate, reducing the cost of coal washing, and realizing the efficient and clean utilization of coal [24, 25].

Nevertheless, based on the above review, only a few have focused on the fundamental theories of compound dry separator. In this study, the novel compound dry separator (NCDS) was proposed to realize highly efficient dry coal preparation. A dynamics model governing the vibration of the separator was presented, and the kinematics characteristics were systematically analyzed by vibration testing technology and multibody dynamics simulation. Besides, the effects of the eccentricity of the shaft on the vibration characteristics of the separator were investigated parametrically. The study provides theoretical and technical support for research and industrial applications of the novel compound dry separator, leading to low coal slurry production as well as low pollution.

## 2. Model Constructions

As shown in Figure 1, the mechanical structure of the novel compound dry separator (NCDS) is composed of two parts: the air supply system and the main machine system. An air supply system includes an air compressor, an air inlet, an air outlet, and so on. The main machine system of the separator mainly includes the separation bed, the supporting structure, feeding and discharging ports, and the driving system. The supporting structure mainly includes the main frame, power frame, and bed support frame. The separation bed is connected to the eccentric sleeve, bearing, and shaft by a blade spring. The shaft is connected with the counterweight block in the opposite direction through another blade spring, eccentric sleeve, and bearing. The shaft is also fixed on the power bracket through the bearing seat and driven by the motor through the pulley and belt. The driving motor is a frequency conversion motor, which controls the start, stop, and rotational speed. The horizontal and longitudinal inclination angles of the separation bed can be adjusted by the inclination adjustment device. The shaft drives the eccentric shaft sleeve, and the reciprocating movement of the separation bed is driven by the blade spring.

The vibration intensity of the separation bed is closely related to the performance of the NCDS. Therefore, it plays a key role in fully understanding the working performance of the NCDS to reveal the dynamic mechanical characteristics and discuss the vibration behavior of the separator.

When the shaft rotates, the displacement, velocity, and acceleration of the separation bed can be expressed as [26]

$$\begin{cases} x = e \cos \varphi \cos \omega t, \\ y = e \sin \varphi \cos \omega t, \end{cases} \quad (1)$$

$$\begin{cases} \dot{x} = -e\omega \cos \varphi \sin \omega t, \\ \dot{y} = -e\omega \sin \varphi \sin \omega t, \end{cases} \quad (2)$$

$$\begin{cases} \ddot{x} = -e\omega^2 \cos \varphi \cos \omega t, \\ \ddot{y} = -e\omega^2 \sin \varphi \cos \omega t, \end{cases} \quad (3)$$

where  $(x, y)$ ,  $(\dot{x}, \dot{y})$ , and  $(\ddot{x}, \ddot{y})$  are the displacement, velocity, and acceleration, respectively, of the separation bed along the  $X$  and  $Y$  directions.  $\varphi$  is the included angle between the blade spring and the separation bed,  $e$  is eccentricity, and  $\omega$  is the angular rotational speed of the shaft.

## 3. Experiment Set up

The experiment and analysis system for dynamic characteristics of the NCDS is shown in Figure 2. The system mainly includes a circuit breaker, a frequency converter, the NCDS, an ICP three-direction acceleration sensor, an INV3060S multichannel signal acquisition instrument, and Coinv DASP multichannel signal real-time analysis software.

The circuit breaker controls the opening and closing of the entire circuit. The frequency converter is used to set the output speed of the variable frequency motor. The three-direction acceleration sensor is connected with the multichannel acquisition instrument through a cable. The  $X$ -direction of the acceleration sensor is parallel to the surface of the separation bed; the  $Y$ -direction is perpendicular to the surface of the separation bed; and the  $Z$ -axis direction is perpendicular to the side plate. The multichannel acquisition device is connected to a computer installed with Coinv DASP software through a network cable.

The sampling time should be set for at least 1 minute in order to record the acceleration signals at different stages completely. At the same time, in order to ensure the reliability of the test data, the same working conditions need to be repeated three times. The acceleration signal collected by the sensor is transmitted to the computer through a cable, multichannel data acquisition instrument, and network cable, and then analyzed in time and frequency domain by DASP software.

## 4. Results and Discussion

*4.1. Kinetic Analysis of the NCDS based on Multibody Dynamics.* Through the theoretical model, the dynamic parameters of the NCDS can be obtained. In order to study the correctness and feasibility of the analysis method more accurately, the motion characteristics of the NCDS are simulated and analyzed by the multi-body dynamics software ADMAS. Through this software, different parameters, such as displacement, velocity, and acceleration, can be obtained. In the process of modeling, the mechanical structure was simplified.

In the ADAMS software interface, a simplified simulation model of the NCDS was established, as shown in Figure 3. The eccentricity  $e$  is 8 mm and the plate spring inclination  $\varphi$  is 30°.

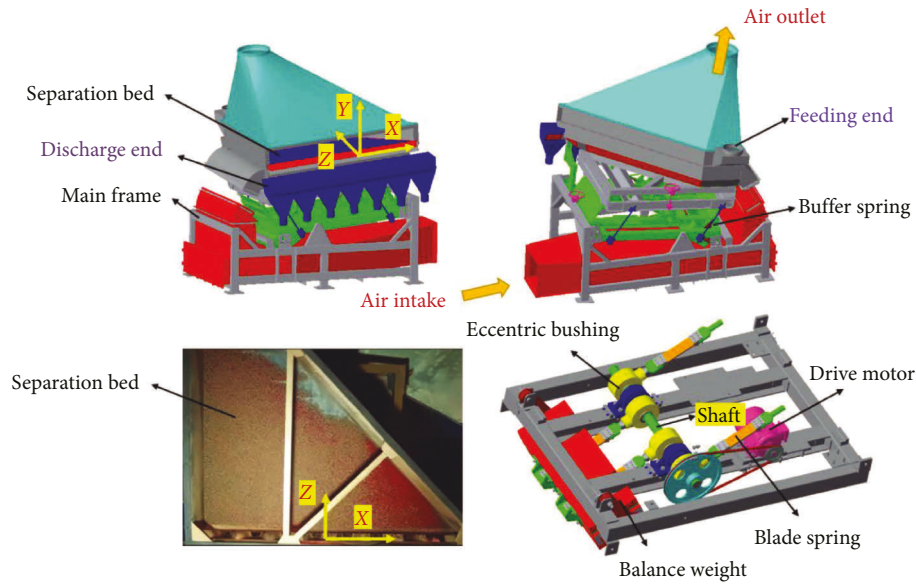


FIGURE 1: Structure of the novel compound dry separator (NCDS).

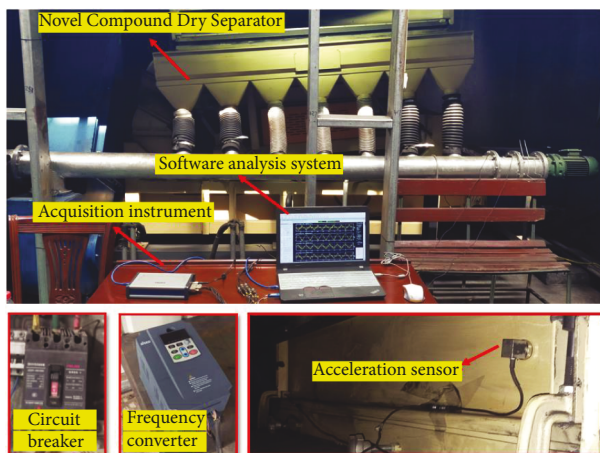


FIGURE 2: Arrangement of the experiment and analysis system.

The spring stiffness was set according to the theoretical calculation. The structure material chosen was steel, with a corresponding density of  $7.82 \times 10^3 \text{ kg}\cdot\text{m}^{-3}$ . The restraint formed between the shaft and eccentric sleeve, eccentric sleeve and plate spring, and plate spring and separation bed were defined as joint rotation pairs. Apply motion rotation drive to the joint rotation pair between the mandrel and eccentric sleeve. The motion speed function was set as follows: STEP (time, 0, 0,  $t_0$ ,  $\omega_0$ ), that is, in the first  $t_0$  second, the speed increases from 0 to  $\omega_0$ . After  $t_0$  seconds, the shaft moves in a uniform circular motion. In this study,  $t_0$ ,  $\omega_0$ , and total simulation times were 10 s,  $38.7 \text{ rad}\cdot\text{s}^{-1}$  (370 rpm), and 20 s, respectively. The step size of the simulation was set to 0.002 s to record experimental data every 0.002 s.

Figure 4 shows the time-domain response curve of the separation bed displacement. It can be seen from Figure 4(a) that during 0–10 s, the NCDS is in the starting stage, and the vibration frequency of the bed gradually accelerates. After 10 s, the bed is in a stable operation state. Figure 4(b) shows

the time-domain response curves of bed displacement along X and Y directions under stable operation. Under stable operation, the displacement of the separation bed is harmonic, and the displacement phase difference is always 0. At this time, the displacement amplitude of the separation bed in the X-direction is 7.01 mm, and the displacement amplitude in the Y-direction is 3.84 mm.

Figure 5 shows the time-space characteristic curve and the displacement Lissajous figure obtained according to the time-domain response of displacement. The time-space characteristic curves show that the space displacement of the separation bed is chaotic at first and then stable slowly. In a stable operation state, the Lissajous figure shows that the displacement track of the separation bed is an inclined straight line.

Figure 6 shows the time-domain response curve of the separation bed velocity. As can be seen from Figure 6(a), in the first stage (0 to 10 s), the velocity amplitude  $|\dot{x}|$  and  $|\dot{y}|$  increases gradually. After 10 s, velocity amplitude stays stable. Figure 6(b) shows that during steady-state, the velocity amplitude  $|\dot{x}|$  is  $271.7 \text{ mm}\cdot\text{s}^{-1}$  and the velocity amplitude  $|\dot{y}|$  is  $149.3 \text{ mm}\cdot\text{s}^{-1}$ . In steady operation, the velocity of  $\dot{x}$  and  $\dot{y}$  run in the same direction.

Figure 7 shows the time-domain response curve of the separation bed acceleration. As can be seen from Figure 7(a), during the start-up stage (0–10 s), the acceleration amplitude of the separation bed along the X and Y directions gradually increases, and after 10 s, the amplitude reaches its maximum and starts to run steadily. It can be seen from Figure 7(b) that the acceleration amplitude of the separation bed in the stable state is  $10.6 \text{ m}\cdot\text{s}^{-2}$  in the X direction and  $6.0 \text{ m}\cdot\text{s}^{-2}$  in the Y direction. Under stable operation, the direction of acceleration is always the same.

Table 1 shows the comparisons such as displacement amplitude, velocity amplitude, and acceleration amplitude between the theoretical calculation results based on the dynamic model and the simulation results based on

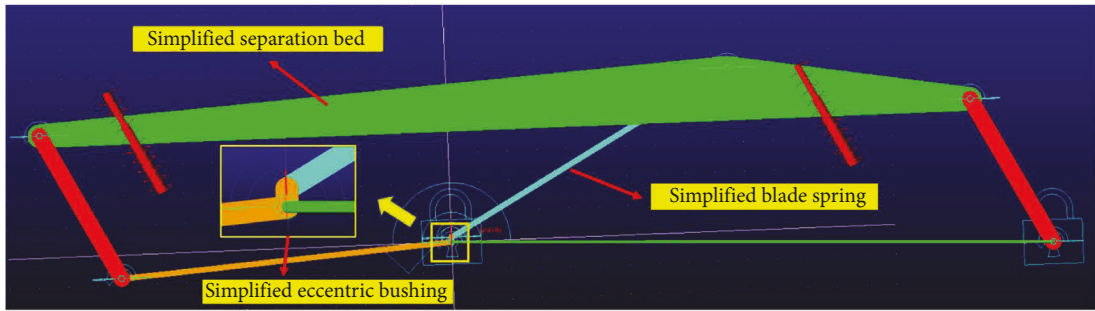


FIGURE 3: Simulation model of the NCDS.

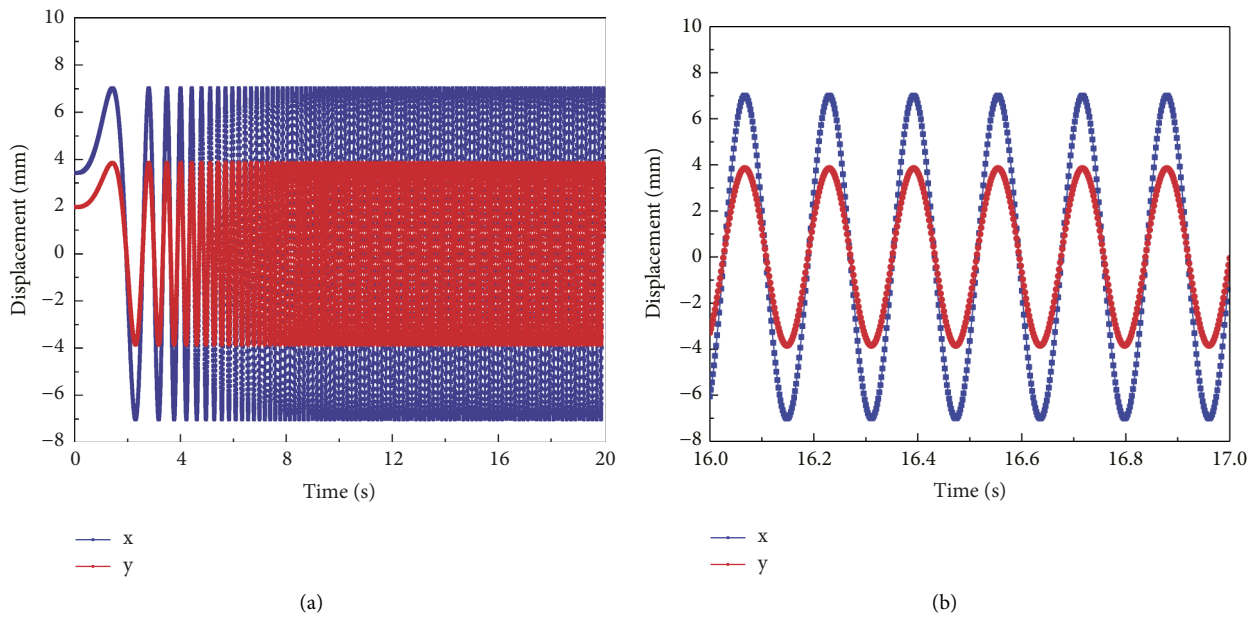


FIGURE 4: Time-responses of the displacement about the NCDS.

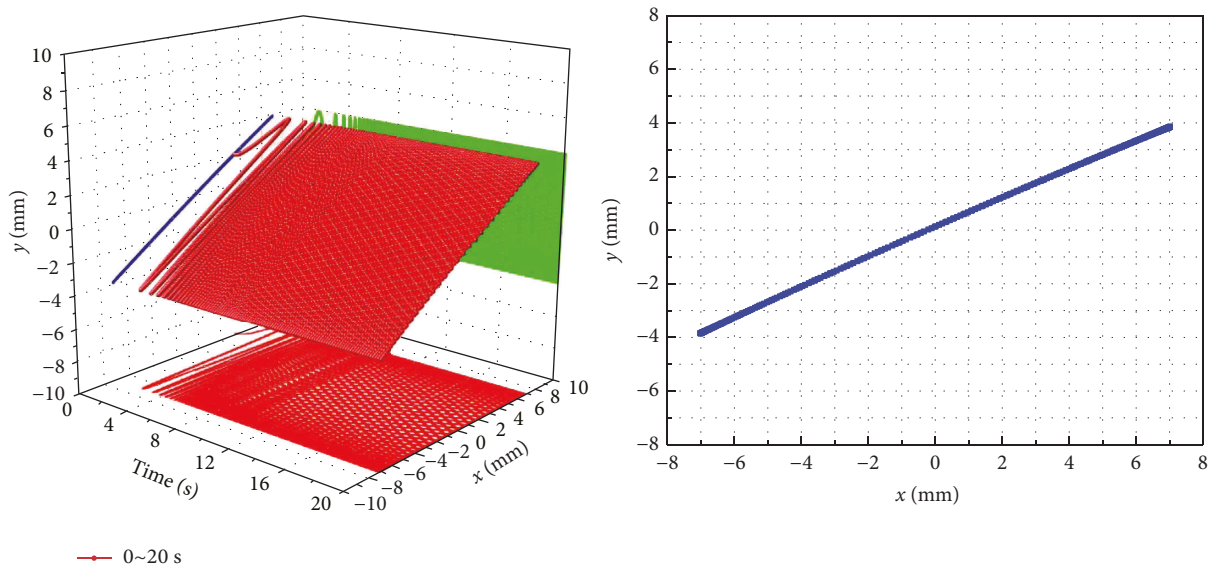


FIGURE 5: Space-time curve and Lissajous figure of displacement about the NCDS.

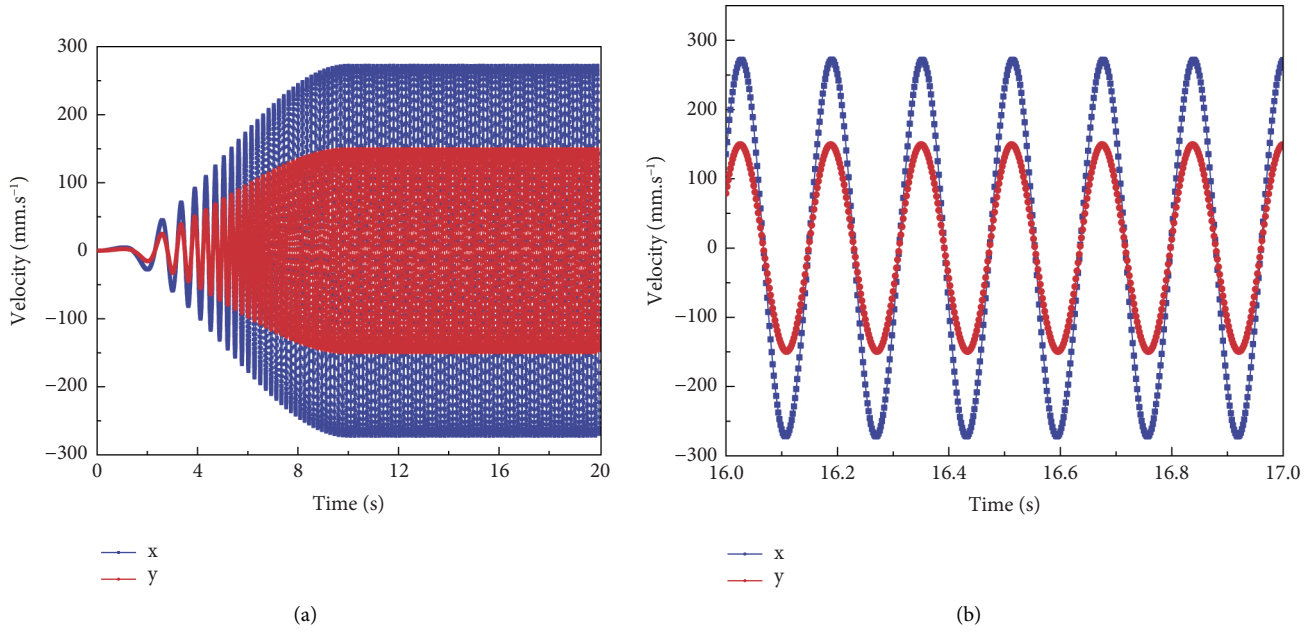


FIGURE 6: Time-responses of the velocity about the NCDS.

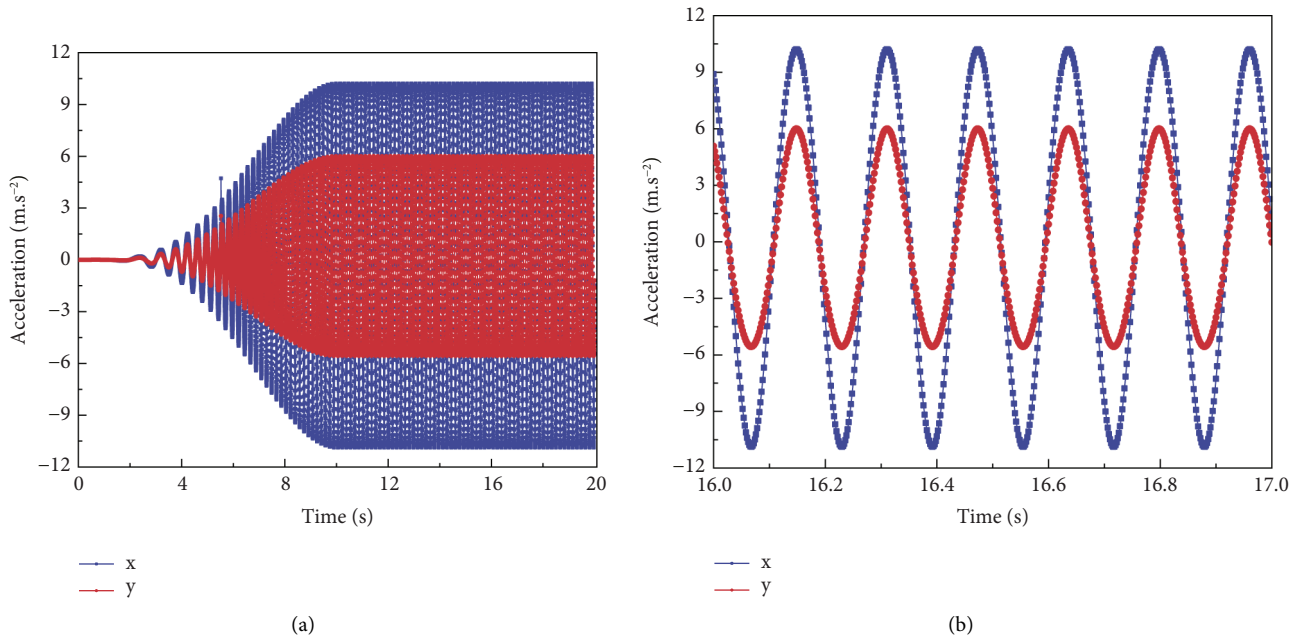


FIGURE 7: Time-responses of the acceleration about the NCDS.

TABLE 1: Comparisons of theoretical results and simulation results.

Parameters	Theoretical results	Simulation results	Error (%)
$ x $ (mm)	6.93	7	1.01
$ \dot{x} $ (mm.s <sup>-1</sup> )	268.1	271.7	1.34
$ \ddot{x} $ (m.s <sup>-2</sup> )	10.4	10.6	1.92
$ y $ (mm)	4.0	3.85	-3.75
$ \dot{y} $ (mm.s <sup>-1</sup> )	154.7	149.3	-3.49

multibody dynamics (MBD) of the motion characteristics of the separation bed of the NCDS. It can be seen that the simulation results are in good agreement with the theoretical

calculation results. The maximum relative error is only 3.75%. It shows that the theoretical calculation results have high reliability and accuracy.

#### 4.2. Vibration Analysis Based on the Dynamic Experiment.

Based on the theoretical model, it can be found that the vibration characteristics of the separation bed are related to the shaft rotational speed. The shaft rotational speed is determined by the driving motor. The frequency of the current determines the rotational speed of the driving motor. In order to study the influence of shaft rotational speed on the vibration performance of the NCDS, the frequency converter parameters were set to 36.7, 38.6, 40.7, 42.6, and 44.7 Hz, respectively, and the corresponding angular speed  $\omega$  of shaft rotational speed was 38.74, 40.75, 42.97, 43.2.97, and 47.19  $\text{rad}\cdot\text{s}^{-1}$ , respectively. That is, the shaft rotational speeds  $n$  are 370.16, 389.33, 410.51, 429.67, and 450.85 rpm, respectively.

Experimental test results and theoretical results about dynamic characteristics under different rotational speeds of the separation bed along the  $X$ -direction are shown in Figure 8. Generally, with the increase of the rotational speed  $n$ , the displacement amplitude along the  $X$ -direction is basically unchanged, while the velocity amplitude and acceleration amplitude gradually increase. Figure 8(a) shows the variation tendency of the displacement amplitude of the separation bed along the  $X$ -direction under stable working conditions. It can be seen that the displacement amplitude increases slightly with the increase of the rotational speed  $n$ . When the speed  $n$  increases from 370.16 to 410.51 rpm, the displacement amplitude of the separation bed along the  $X$ -direction increases from 6.88 mm to 7.30 mm. When  $n$  further increases to 450.85 rpm, the displacement amplitude continues to increase to 7.40 mm. At different rotational speeds, the displacement amplitudes are always about 7 mm, which is equal to  $e\cdot\cos\varphi$ .

Figure 8(b) shows the change rule of the velocity amplitude along the  $X$ -direction under stable working conditions. It can be seen that the velocity amplitude increases with the increase of the motor speed  $n$ . When the speed  $n$  increases from 370.16 to 410.51 rpm, the velocity amplitude increases from  $286.8\text{ mm}\cdot\text{s}^{-1}$  to  $316.2\text{ mm}\cdot\text{s}^{-1}$ . When the speed  $n$  continues to increase to 450.85 rpm, the velocity amplitude increases to  $349.2\text{ mm}\cdot\text{s}^{-1}$ . The velocity amplitude along the  $X$ -direction is  $e\cdot\omega\cdot\cos\varphi$  approximately with different rotational speeds.

Figure 8(c) shows the acceleration curve of the separation bed along the  $X$ -direction. When the speed  $n$  increases from 370.16 to 450.85 rpm, the acceleration amplitude along the  $X$ -direction of the separation bed increases from  $10.43\text{ m}\cdot\text{s}^{-2}$  to  $16.46\text{ m}\cdot\text{s}^{-2}$ . The acceleration amplitudes in the  $X$ -direction are always equal to  $e\cdot\omega^2\cdot\cos\varphi$ . The experimental results are in good agreement with the theoretical ones along the  $X$ -direction.

The dynamic characteristics along the  $Y$ -direction are shown in Figure 9. With the increase of the rotational speed  $n$ , the displacement amplitude in the  $Y$ -direction increases slightly, while the velocity amplitude and acceleration amplitude increase gradually. Figure 9(a) shows the variation tendency of the displacement amplitude of the separation bed along the  $Y$ -direction under stable working conditions. When the rotational speed  $n$  increases from 370.16 to 410.51 rpm, the displacement amplitude increases from

3.78 mm to 4.10 mm. When  $n$  further increases to 450.85 rpm, the displacement amplitude continues to increase to 4.25 mm. At different rotational speeds, the displacement amplitude of the separator surface along the  $Y$ -direction is always about 4 mm, which is equal to  $e\cdot\sin\varphi$ .

Figure 9(b) shows the change of velocity amplitude of the separation bed along the  $Y$ -direction under stable working conditions. It can be seen from the figure that the speed amplitude of the separation bed surface along the  $Y$ -direction increases with the increase in the rotational speed  $n$ . When the speed  $n$  increases from 370.16 to 410.51 rpm, the velocity amplitude increases from  $161.6\text{ mm}\cdot\text{s}^{-1}$  to  $183.1\text{ mm}\cdot\text{s}^{-1}$ . When the speed  $n$  continues to increase to 450.85 rpm, the velocity amplitude increases to  $191.2\text{ mm}\cdot\text{s}^{-1}$ . The velocity amplitude in the  $Y$ -direction is approximately equal to  $e\cdot\omega\cdot\sin\varphi$  at different rotational speeds. Figure 9(c) shows the acceleration curve along the  $Y$ -direction. When the speed  $n$  increases from 370.16 to 450.85 rpm, the acceleration amplitude of the separation bed increases from  $5.92\text{ m}\cdot\text{s}^{-2}$  to  $9.45\text{ m}\cdot\text{s}^{-2}$ . The acceleration amplitudes along the  $Y$ -direction are always equal to  $e\cdot\omega^2\cdot\sin\varphi$ .

It should be noted that when  $n$  increases from 370.16 rpm to 450.85 rpm, the displacement amplitude of the separation bed along the  $X$ -direction increases by only 7.55%, while the velocity amplitude and acceleration amplitude increase by 21.75% and 57.81%, respectively. Similarly, the displacement amplitude in the  $Y$ -direction increased by 12.43%, while the velocity amplitude and acceleration amplitude increased by 18.32% and 59.63%, respectively. When the speed  $n$  exceeds a certain range, further increasing  $n$  will increase the displacement amplitude of the bed surface rapidly, especially the velocity and acceleration amplitude of the separation bed. Therefore, the rotational speed should be controlled within a certain range.

It can also be seen from Figures 8 and 9 that the experimental results of the dynamic characteristics of the separation bed surface of the NCDS have a strong consistency with the theoretical results. The relative error between experimental results and theoretical results is less than 7%, with a maximum error of 6.98%. The experimental results show that the kinetic theory model of the new type of dry separator can describe its motion mechanism perfectly.

#### 4.3. Vibration Characteristics with Different Eccentricities.

After the prototype was made, the eccentricity was not adjustable. Therefore, in this section, the influence of eccentricity  $e$  on the dynamic characteristics of the NCDS is discussed through theoretical analysis. Table 2 describes the parameters and their values. The angle between the plate spring and the separation bed  $\varphi$  is  $30^\circ$ , and the angular rotational speed of the shaft  $\omega$  is  $43\text{ rad}\cdot\text{s}^{-1}$  (equivalent to rotational speed  $n = 410.5\text{ rpm}$ ). According to Equations (1)–(3), the vibration characteristics of the separation bed are proportional to the eccentricity  $e$ . When the eccentricity  $e$  is 4, 8, and 12 mm, the displacement ( $x, y$ ), velocity ( $\dot{x}, \dot{y}$ ), and acceleration ( $\ddot{x}, \ddot{y}$ ), as shown in Figure 10. It can be found that the displacement amplitude  $|x|, |y|$ , velocity

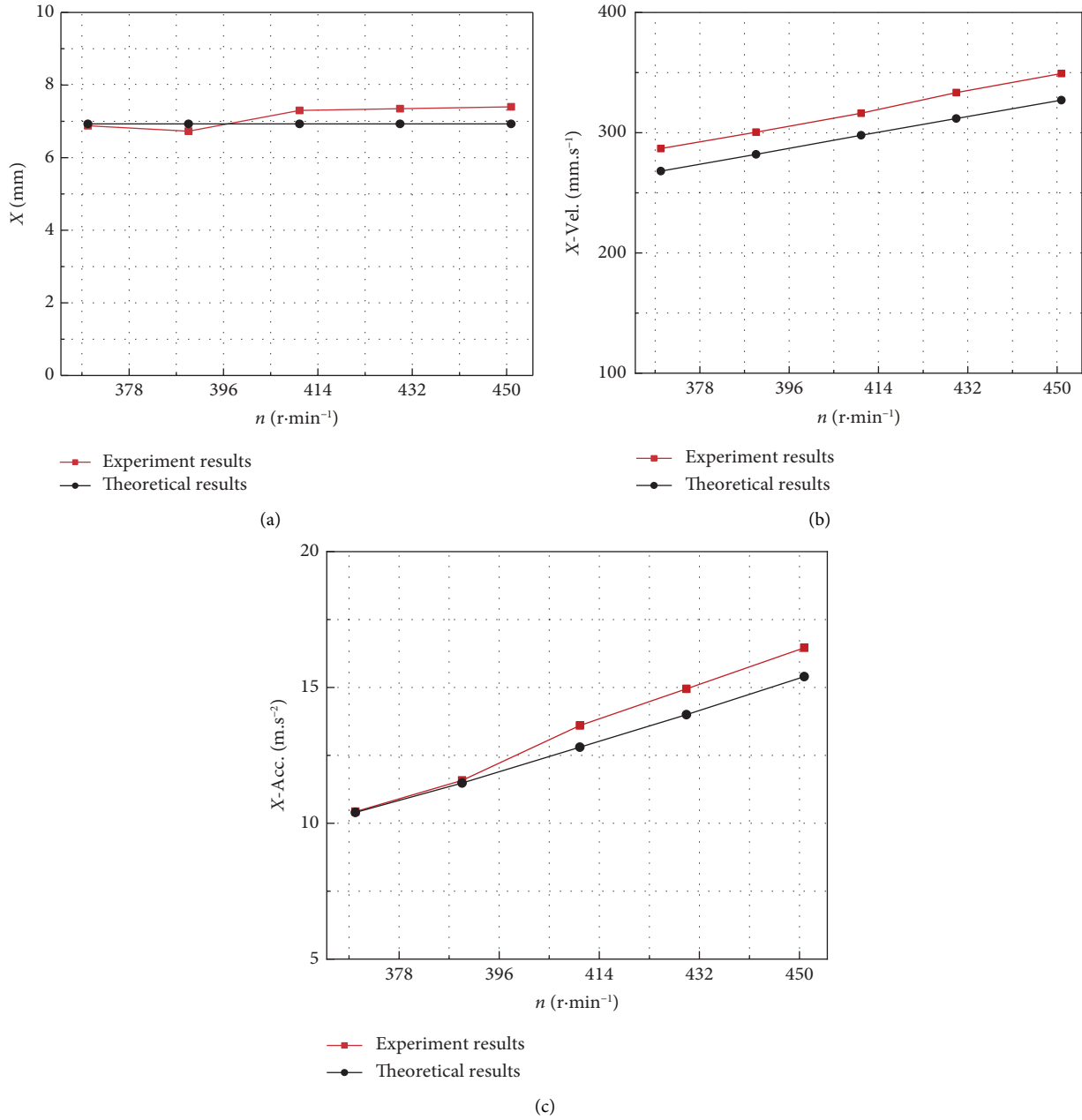


FIGURE 8: Dynamic characteristics along X-direction under different rotational speed between experiments and theoretical calculations.

amplitude  $|\dot{x}|$ ,  $|\dot{y}|$ , and acceleration amplitude  $|\ddot{x}|$ ,  $|\ddot{y}|$  are increased with the increase of eccentricity  $e$ .

As shown in Figure 10(a), in the first half cycle (0–0.075 s), the separation bed moves from the maximum forward direction to the minimum negative direction; in the latter half cycle (0.075–0.15 s), the separation bed moves from negative to minimum to positive. As the eccentricity  $e$  increases from 4 mm to 12 mm, the separation bed displacement amplitude of X-direction  $|x|$  increases from 3.46 mm to 10.39 mm. Similarly, as shown in Figure 10(b), in the first half period (0–0.075 s), the displacement  $y$  in the Y-direction moves from the maximum in the positive direction to the minimum in the negative direction; in the second half

period (0.075–0.15 s), the displacement  $y$  in the Y-direction moves from the minimum in the negative direction to the maximum in the positive direction. As the eccentricity  $e$  increases from 4 mm to 12 mm, the displacement amplitude  $|y|$  increases from 2.0 mm to 6.0 mm.

In addition, appropriately increasing the amplitude of motion velocity and acceleration will increase the possibility of particle stratification on the bed surface. We can see from Figures 10(c) and 10(d) that as eccentricity  $e$  increases from 4 mm to 12 mm, the X-direction velocity amplitude  $|\dot{x}|$  of the separation bed increases from 148.5 mm.s<sup>-1</sup> to 445.6 mm.s<sup>-1</sup>, while Y-direction velocity amplitude  $|\dot{y}|$  increases from 85.7 mm.s<sup>-1</sup> to 257.1 mm.s<sup>-1</sup>. From Figures

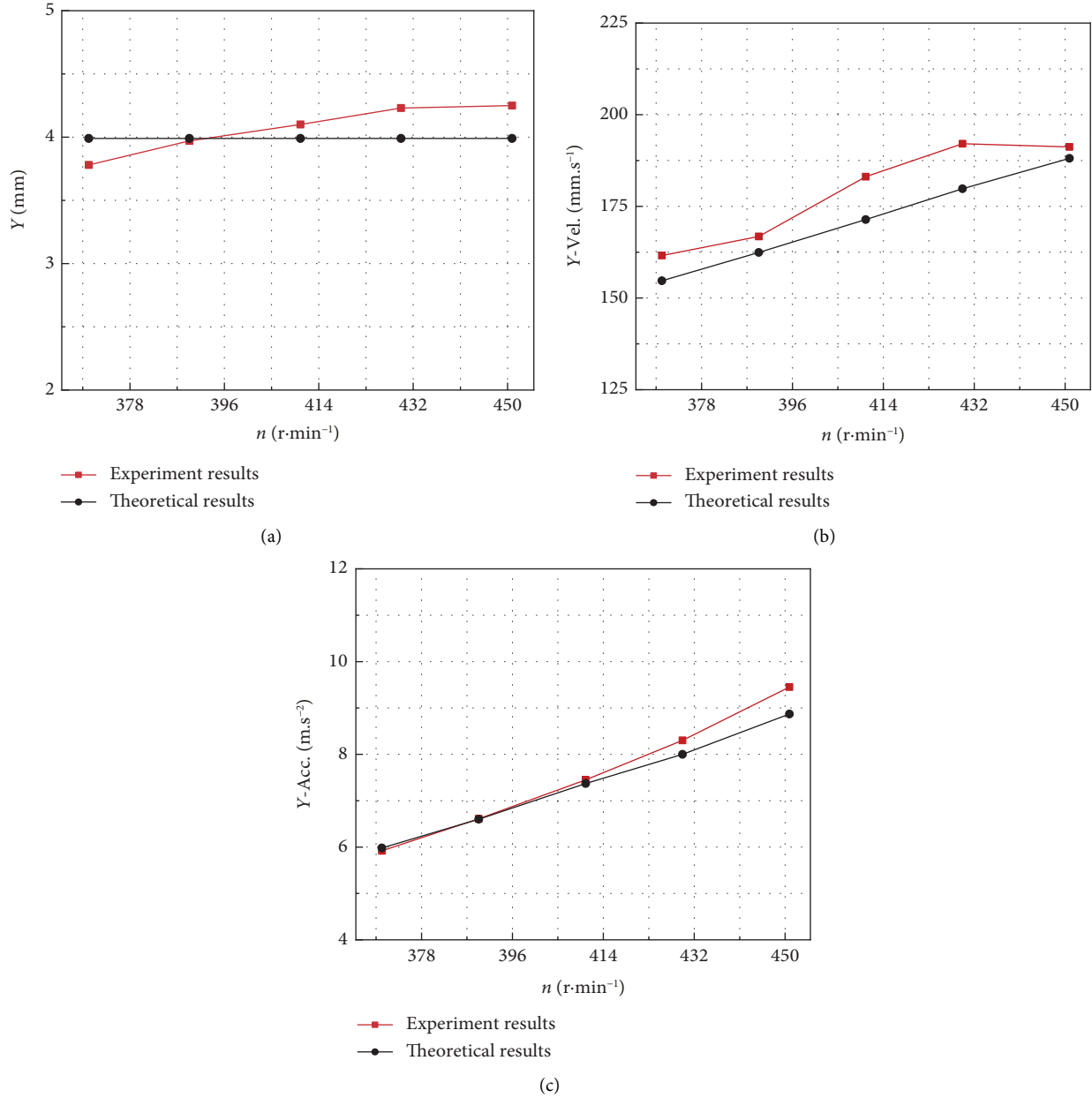


FIGURE 9: Dynamic characteristics along Y-direction under different rotational speed between experiments and theoretical calculations.

TABLE 2: Parameters used in section 4.3.

Item	Value
$\varphi$ (°)	30
$\omega$ (rad.s <sup>-1</sup> )	43 ( $n = 410.5$ rpm)
$e$ (mm)	4
	8
	12

10(e) and 10(f), we can see that separation bed X-direction acceleration amplitude  $|\ddot{x}|$  increased to  $19.2 \text{ m}\cdot\text{s}^{-2}$  from  $6.4 \text{ m}\cdot\text{s}^{-2}$ ; Y-direction acceleration amplitude  $|\ddot{y}|$  increased from  $3.7 \text{ m}\cdot\text{s}^{-2}$  to  $11.1 \text{ m}\cdot\text{s}^{-2}$ . At the same time, high speed and acceleration will reduce the time duration of the particles on the bed, which is not conducive to sorting. Therefore, a reasonable choice of eccentricity is necessary.

Because the eccentricity cannot be adjusted, the effect of eccentricity can only be analyzed theoretically. Through theoretical analysis, the designer can understand and grasp the principle of eccentricity on the vibration characteristics of the NCDS. The discussion on eccentricity provides a theoretical basis for the further development of the separation machine.



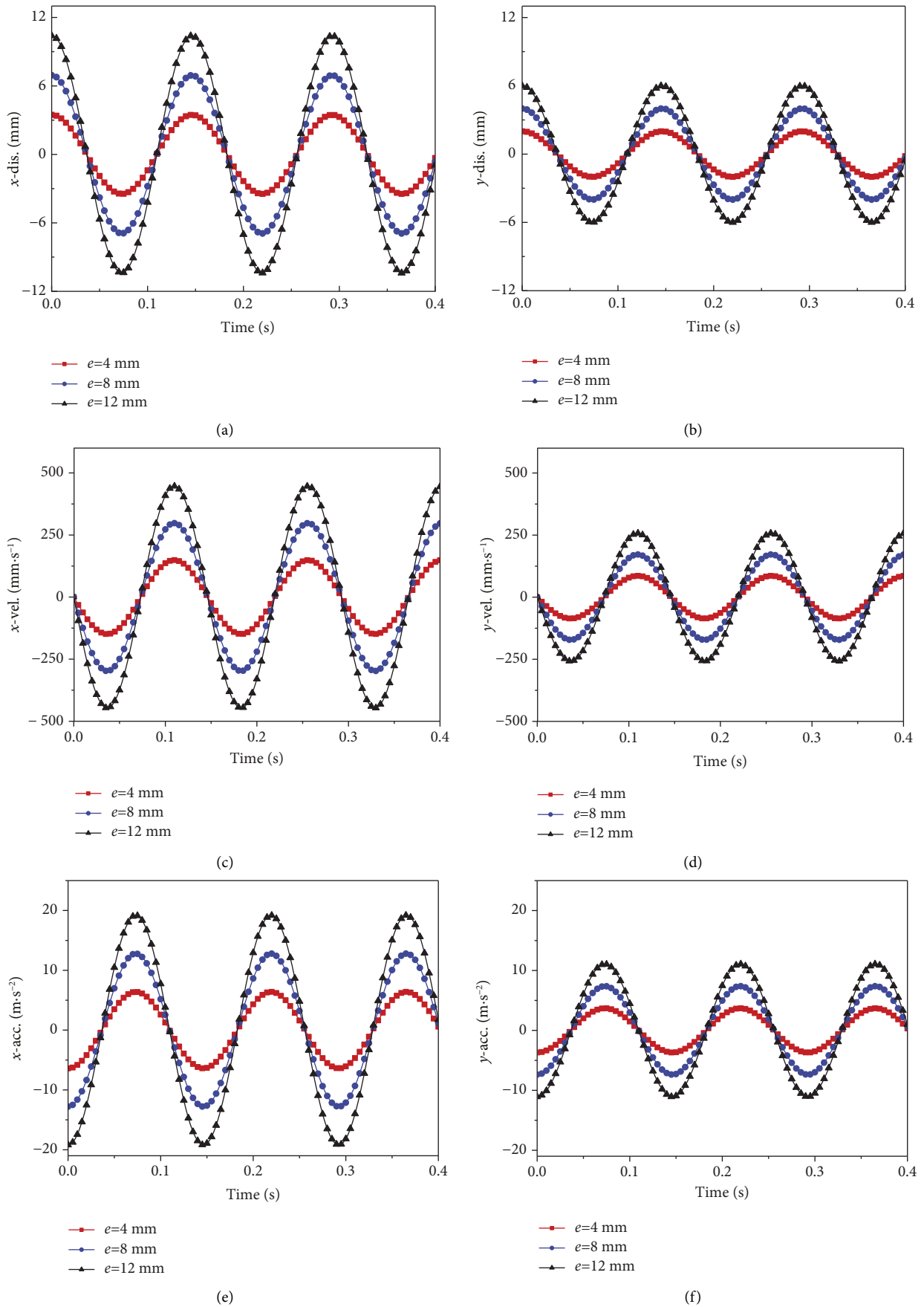


FIGURE 10: Kinematic characteristics of the NCDS with different eccentricity  $e$  (a), (b) displacement  $(x, y)$ ; (c), (d) velocity  $\dot{x}, \dot{y}$ ; and (e), (f) acceleration  $\ddot{x}, \ddot{y}$ .

## 5. Conclusions

- (1) The mechanical structure and dynamic model of the novel compound dry separator (NCDS) were established. Through theoretical analysis, the dynamics characteristics of the NCDS, including the amplitude of displacement, velocity, and acceleration, all increase with the increase of eccentricity. With the increase in the shaft rotational speed, the displacement amplitude remains unchanged, and the amplitude of the velocity and acceleration increase gradually.
- (2) Based on the multibody dynamics analysis, a virtual prototype model of the NCDS was established, and the simulation was carried out. The vibration behavior of the NCDS was studied, such as motion curve, space trajectory, and displacement Lissajous figure. The space motion trajectory of the NCDS was an oblique line. The theoretical calculation results were compared with the simulation results. The comparison results show that the simulation results are in good agreement with the theoretical ones, and the maximum relative error was less than 3.75%.
- (3) The vibration experiment system was carried out. The dynamic characteristics, including displacement, velocity, and acceleration in  $X$  and  $Y$  directions of the NCDS under different rotational speeds, were obtained. The experiment results were compared with the theoretical results. The maximum error between experimental results and theoretical results was 6.98%. The temporal and spatial characteristics of the NCDS were revealed, and the validity and accuracy of the theoretical model were proved.

## Data Availability

The raw data required to reproduce these findings cannot be shared at this time, as the data also form part of an ongoing study.

## Additional Points

The mechanical structure and dynamic models of a novel compound dry separator were proposed. The dynamics analysis of the NCDS was performed by means of MBD. The vibrations of the NCDS were examined by experiment and compared with the theoretical calculation. The effects of key parameters on the dynamics of the NCDS were analyzed.

## Conflicts of Interest

The authors declare that they have no conflicts of interest.

## Acknowledgments

This work is financially supported by the National Natural Science Foundation of China (51904298) and the Doctoral Scientific Research Foundation of Suzhou University (2020BS004).

## References

- [1] C. Sheng, C. L. Duan, Y. M. Zhao, P. P. Zhang, and L. Dong, "Separation and upgrading of fine lignite in a Pulsed fluidized bed. 2. Experimental study on lignite separation characteristics and Improvement of separation efficiency," *Energy & Fuels*, vol. 32, no. 1, pp. 936–953, 2018.
- [2] C. Sheng, C. L. Duan, Y. M. Zhao, P. P. Zhang, and L. Dong, "Separation and upgrading of fine lignite in Pulsed fluidized bed. 1. Experimental study on lignite drying characteristics and kinetics," *Energy & Fuels*, vol. 32, no. 1, pp. 922–935, 2018.
- [3] D. Li, D. S. Wu, F. G. Xu, J. H. Lai, and L. Shao, "Literature overview of Chinese research in the field of better coal utilization," *Journal of Cleaner Production*, vol. 185, pp. 959–980, 2018.
- [4] J. Wu, C. Liu, and Z. Wang, "Numerical simulation of dynamic characteristics and parameter optimization of flip-flow screen surface," *Journal of Central South University*, vol. 50, no. 02, pp. 311–320, 2019.
- [5] A. Noble and G. H. Luttrell, "A review of state-of-the-art processing operations in coal preparation," *International Journal of Mining Science and Technology*, vol. 25, no. 4, pp. 511–521, 2015.
- [6] M. Kademli and O. Y. Gulsoy, "Investigation of using table type Air separators for coal cleaning," *International Journal of Coal Preparation and Utilization*, vol. 33, no. 1, pp. 1–11, 2013.
- [7] G. Huang, J. T. Liu, L. J. Wang, and Z. H. Song, "Flow field simulation of agitating tank and fine coal conditioning," *International Journal of Mineral Processing*, vol. 148, pp. 116–123, 2016.
- [8] A. R. Liu, J. C. Gao, and M. Q. Fan, "Performance of an air-injected water-only Cyclone for the separation of fine coal," *International Journal of Coal Preparation and Utilization*, vol. 33, no. 5, pp. 218–224, 2013.
- [9] Y. Xuliang, Z. Yuemin, L. Gongmin, L. Zhenfu, C. Zengqiang, and L. Chunheng, "Establishment and Evaluation of a united dry coal beneficiation system," *International Journal of Coal Preparation and Utilization*, vol. 32, no. 2, pp. 95–102, 2012.
- [10] Y. Xiaodong, L. Zhenfu, G. Deqing, and L. Gongmin, "Upgrading of lignite using a combined novel drying and the FGX dry separation process," *International Journal of Coal Preparation & Utilization*, vol. 41, pp. 343–361, 2018.
- [11] R. K. Dwari and K. H. Rao, "DRY beneficiation of coal—a review," *Mineral Processing and Extractive Metallurgy Review*, vol. 28, no. 3, pp. 177–234, 2007.
- [12] X. Ling, Y. He, Y. Zhao, G. Li, J. Wang, and B. Wen, "Distributions of size, Ash, and density of coal particles along the Front Discharge section of a compound dry separator," *International Journal of Coal Preparation and Utilization*, vol. 38, no. 8, pp. 422–432, 2018.
- [13] J. Haishen, Yu Shijie, H. Long et al., "Kinematics and mechanism of rigid-flex elastic screening for moist coal under disequilibrium excitation," *International Journal of Coal Preparation and Utilization*, vol. 42, pp. 1724–1739, 2020.
- [14] H. Li, C. Liu, L. Shen, L. Zhao, and S. Li, "Kinematics characteristics of the flip-flow screen with a crankshaft-link structure and screening analysis for moist coal," *Powder Technology*, vol. 394, pp. 326–335, 2021.
- [15] X. Yang, Y. Zhao, Z. Luo, S. Song, C. Duan, and L. Dong, "Fine coal dry cleaning using a vibrated gas-fluidized bed," *Fuel Processing Technology*, vol. 106, pp. 338–343, 2013.
- [16] X. Yang, Y. Zhao, Z. Luo, S. Song, and Z. Chen, "Fine coal dry beneficiation using autogenous medium in a vibrated

- fluidized bed,” *International Journal of Mineral Processing*, vol. 125, pp. 86–91, 2013.
- [17] Z. F. Luo, L. G. Tang, N. N. Dai, and Y. M. Zhao, “The effect of a secondary gas-distribution layer on the fluidization characteristics of a fluidized bed used for dry coal beneficiation,” *International Journal of Mineral Processing*, vol. 118, pp. 28–33, 2013.
- [18] Y. Yang and G. Li, “Development and application of large complex dry coal preparation equipment,” *Coal Preparation Technology*, vol. 4, pp. 47–50, 2008.
- [19] N. Fraunholz, “Separation of waste plastics by froth flotation--a review, part I,” *Minerals Engineering*, vol. 17, no. 2, pp. 261–268, 2004.
- [20] X. Yu, Z. Luo, H. Li, and D. Gan, “Beneficiation of 6-0mm fine-grain oil shale using vibrating air-dense medium fluidized bed separator,” *Fuel*, vol. 203, pp. 341–351, 2017.
- [21] L. Shen, “Role of authigenic medium in compound dry separator,” *Coal Preparation Technology*, vol. 2, pp. 45–48, 1998.
- [22] J. Liu, X. Li, and Y. Wang, “Experimental study on separating some molybdenum ore by using cyclonic-static micro-bubble flotation column,” *Journal of Central South University*, vol. 39, no. 2, pp. 300–306, 2008.
- [23] L. Shen and J. Chen, “Analysis of Material motion in compound dry separator,” *Journal of China University of Mining and Technology*, vol. 34, no. 4, pp. 447–451, 2005.
- [24] J. Haishen, W. Pengfei, L. Zhenfu et al., “Optimization of the disequilibrium excitation rigid-flex elastic screening process and its application for coal beneficiation,” *International Journal of Coal Preparation and Utilization*, vol. 42, pp. 1460–1476, 2020.
- [25] B. C. Song, C. S. Liu, L. P. Peng, and J. Li, “Dynamic analysis of new type elastic screen surface with multi degree of freedom and experimental validation,” *Journal of Central South University*, vol. 22, no. 4, pp. 1334–1341, 2015.
- [26] H. Li, E. Zhou, L. Shen, Z. Yin, and Z. Bo, “Dynamical characteristics and vibration behavior of the novel composite dry separator,” *Vibroengineering PROCEDIA*, vol. 40, pp. 1–6, 2022.